Sensors and Techniques for Observing Coastal Ecosystems

1 author:

Victor Klemas
University of Delaware
256 PUBLICATIONS   **8,646** CITATIONS

Chapter 2
Sensors and Techniques for Observing Coastal Ecosystems

Victor V. Klemas

This chapter reviews the advances in sensor design and related field techniques that are particularly appropriate for coastal ecosystem research and management. Multi-spectral and hyperspectral imagers are available for mapping coastal land cover and concentrations of organic or inorganic suspended particles and dissolved substances in coastal waters. Thermal infrared scanners can map sea surface temperatures accurately and chart coastal currents, while microwave radiometers can measure ocean salinity, soil moisture and other hydrologic parameters. Radar imagers, scatterometers and altimeters provide information on ocean waves, ocean winds, sea surface height and coastal currents. Using airborne LIDAR one can produce bathymetric maps, even in moderately turbid coastal waters. Since coastal ecosystems have high spatial complexity and temporal variability, they frequently have to be observed from both, satellites and aircraft, in order to obtain the required spatial, spectral and temporal resolutions. A reliable field data collection approach using ships, buoys, and field instruments with a valid sampling scheme is required to calibrate and validate the remotely sensed information.

2.1 Introduction

To understand and manage ecosystems, one must monitor and study their biological/physical features and controlling processes. However, obtaining this information for coastal ecosystems is quite challenging since they exhibit extreme variations in spatial complexity and temporal variability. Also, the influence of coastal ecosystems extends well beyond the local scale, and the only realistic means of obtaining data over such large areas is by remote sensing. To accomplish such monitoring accurately and cost-effectively, the design of the monitoring approach must make integrated use of remote sensing and field techniques (Kerr and Ostrovsky 2003).

V.V. Klemas (✉)
College of Marine and Earth Studies, University of Delaware, Newark, DE 19716, USA
e-mail: klemas@udel.edu

Advances in technology and decreases in cost are now making remote sensing (RS) and geographic information systems (GIS) practical and attractive for use in coastal ecosystem management. They are also allowing researchers and managers to take a broader view of ecological patterns and processes. Landscape-level environmental indicators that can be detected by remote sensors are available to provide quantitative estimates of coastal and estuarine habitat conditions and trends. Such indicators include watershed land cover, riparian buffers, wetland losses and fragmentation, marsh productivity, invasive species, beach erosion, water turbidity and chlorophyll concentrations, among others. New satellites, carrying sensors with fine spatial (1–4 m) and spectral (200 narrow bands) resolutions are being launched, providing a capability to more accurately detect changes in coastal habitat and wetland health. Advances in the application of GIS help incorporate ancillary data layers to improve the accuracy of satellite land-cover classification. When these techniques for generating, organizing, storing, and analyzing spatial information are combined with watershed and ecosystem models, coastal planners and managers have a means for assessing the impacts of alternative management practices.

In Sects. 2.2 and 2.3 of this chapter, the reader is introduced to those airborne and spaceborne remote sensors and techniques which are cost-effective for studying and monitoring coastal ecosystems. In Sects. 2.4 and 2.5, case studies are used to illustrate the application of selected remote sensors and techniques to monitor environmental indicators related to coastal wetland health and estuarine water quality. Section 2.6 describes the most important field techniques required for coastal remote sensing projects. Section 2.7 summarizes the main points followed by a list of carefully selected references.

2.2 Remote Sensors

Aerial photography started approximately in 1858 when the famous French photographer, Gaspard Tournachon, obtained the first aerial photographs from a balloon near Paris. Since then, aerial photography has advanced, primarily during war times, to include color infrared films (for camouflage detection) and sophisticated cameras. Aerial photography and other remote sensing techniques are now used successfully in agriculture, forestry, land use planning, fire detection, mapping wetlands and beach erosion, oceanography and many other applications. For instance, in agriculture they have been used for land-use inventories, soil surveys, crop condition estimates, yield forecasts, acreage estimates, crop insect/pest/disease detection, irrigation management, and more recently, precision agriculture (Jensen 2007).

A major advance in aerial remote sensing has been the development of digital aerial cameras (Al-Tahir et al. 2006). Digital photography is capable of delivering photogrammetric accuracy and coverage as well as multispectral data at any user-defined resolution down to 0.1 m ground sampling distance. It provides photogrammetric positional accuracy with multispectral capabilities for image analysis and interpretation. As no chemical film processing is needed, the direct digital

acquisition can provide image data in just a few hours compared to several weeks using the traditional film-based camera. Another advantage over the traditional film is the ability to assess the quality of data taken directly after the flight is completed. Two examples of digital mapping cameras, ADS40 by Leica Geosystems and DMC from Z/I Imaging, were first presented to the market in 2002 to address requirements for extensive coverage, high geometric and radiometric resolution and accuracy, multispectral imagery, and stereo capability (Leica 2002).

Since the 1960s, remote sensing has progressed to include new techniques of information collection that include aircraft and satellite platforms carrying electro-optical and antenna sensor systems (Campbell 2007). Up to that time, camera systems dominated image collection, and photographic media dominated the storage of the spatially varying visible (VIS) and near-infrared (NIR) radiation intensities reflected from the Earth. Beginning in the 1960s, electronic sensor systems were increasingly used for collection and storage of the Earth's reflected radiation, and satellites were developed as an alternative to aircraft platforms.

Advances in electronic sensors and satellite platforms were accompanied by an increased interest and use of electromagnetic radiant energy not only from the VIS and NIR wavelength regions, but also from the thermal infrared (TIR) and microwave regions. For instance, TIR is used for mapping sea surface temperature and microwaves (e.g. radar) are used for measuring sea surface height, currents, waves and winds on a global scale (Martin 2004).

While most geologists, geographers, and other earth scientists are familiar with aerial photography techniques (Sabins 1978, Avery and Berlin 1992), relatively few scientists have had the opportunity to use thermal infrared, radar, and LIDAR data. Since the TIR radiance depends on both the temperature and emissivity of the target, it is difficult to measure land surface temperatures, because the emissivity will vary as the land cover changes. On the other hand, over water the emissivity is known and nearly constant, 98%, approaching the behavior of a perfect blackbody radiator (Ikeda and Dobson 1995). Thus the TIR radiance measured over the oceans will vary primarily with the sea surface temperature (SST) and allow one to determine the SST accurately ($\pm0.5\,^{\circ}\mathrm{C}$), with some atmospheric corrections (Martin 2004, Elachi and van Ziel 2006).

Radar images represent landscape and ocean surface features that differ significantly from those observed by aerial photography or multispectral scanners. A Side-looking Airborne Radar (SLAR) irradiates a swath along the aircraft flight direction by scanning the terrain with radar pulses at right angles to the flight path. Thus the radar image is created by pulse energy reflected from the terrain and represents primarily surface topography. Since radar images look quite different from visible photographs, they require specialized interpretation skills. Radar pulses penetrate only a few wavelengths into the soil, depending on soil moisture, salinity, surface roughness, etc. The range resolution of SLAR depends on the length of the radar pulse which can be made quite short with new electronic techniques. However, the azimuth resolution is limited by the antenna size and altitude, thus preventing SLAR systems to be used on satellites.

Synthetic Aperture Radar (SAR) was specifically developed to provide high resolution images from satellite altitudes. SAR employs the Doppler shift technique to narrow down the azimuth resolution even with a small antenna. Thus range and azimuth resolutions of the order of 10 m are obtainable with SAR mounted on satellite platforms (Radarsat, ERS-2). In oceanography, radar is used not only for imaging the sea surface but also as altimeters to map sea surface height; scatterometers to determine sea surface winds; etc. (Ikeda and Dobson 1995, Martin 2004). Radar can penetrate fog and clouds, making it particularly valuable for emergency applications and in areas where cloud cover persists. Passive microwave radiometers are becoming important for measuring sea surface salinity, soil moisture and a wide range of hydrology related parameters (Burrage et al. 2003, Parkinson 2003).

Airborne LIDAR (Light Detection and Ranging) has become quite useful for topographic and bathymetric mapping. Laser profilers are unique in that they confine the coherent light energy in a very narrow beam, providing pulses of very high peak intensity. This enables LIDARS to penetrate moderately turbid coastal waters for bathymetric measurements or gaps in forest canopies to provide topographic data for digital elevation models (Brock and Sallenger 2000). The water depth is derived by comparing the travel times of the LIDAR pulses reflected from the sea bottom and the water surface.

As shown in Table 2.1, remote sensors can be classified by application, wavelength or active/passive mode. Under applications we have imagers, which produce two-dimensional images and can be used for map-making. Radiometers measure the radiant energy in a few specific bands, while spectrometers provide the energy distribution across a spectral continuum or many spectral bands. Profilers, such as radar and LIDAR, measure the distance to features, allowing us to determine the topography or bathymetry of an area. Radar and LIDAR are primarily active devices, while most other sensors are passive. The passive sensors operate in three major wavelength regions, the visible, infrared and microwave (Fig. 2.1). In electro-optical multispectral sensors, the visible region is divided into many bands, whereas aerial photography uses blue, green and red bands, plus one reflected band in the near-infrared. Figure 2.2 illustrates different types of visible and infrared imaging

Table 2.1 Classification of remote sensors

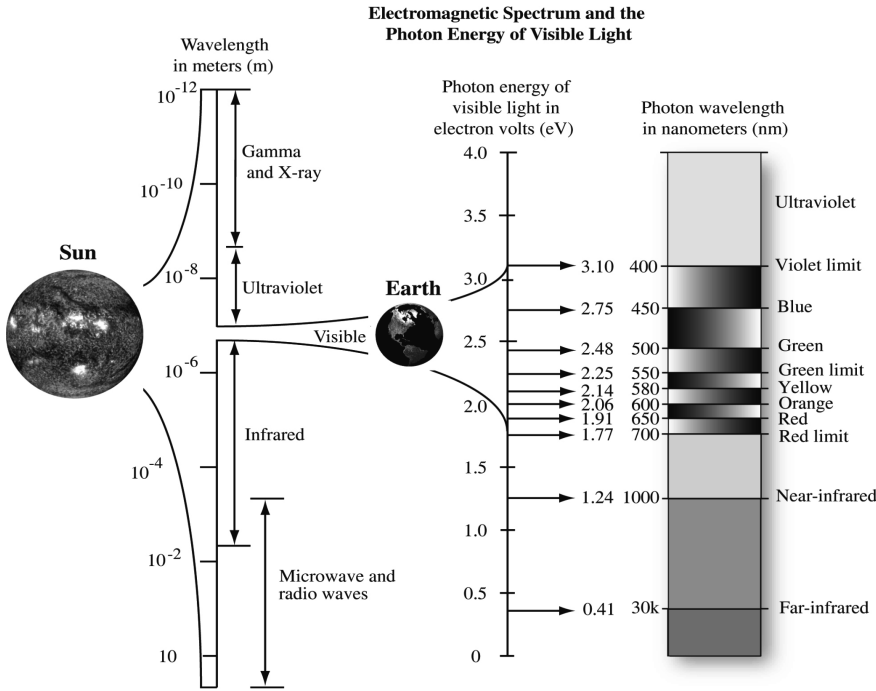| Application	Wavelength	Mode
Imagers (Mappers)	Visible	
Photographic (Film)	Near infrared (Reflected)	Active
Multispectral (Array)	Thermal Infrared (Emitted)	Lidar
Radar (SAR & SLAR)	Microwave	Radar
Side-scanning sonar*	Sound Waves*	Sonar*
Radiometers	Seismic Waves*	
Spectrometers		
Profilers (Rangers)		Passive
Lidar		Visible
Radar (Altimeter)		Infrared
Echo Sounder*		Microwave

*Not electromagnetic (EM) waves.

Fig. 2.1 Electromagnetic spectrum (Jensen 2007)

sensors, including a framing camera; two types of multispectral scanners, the cross-track or whisk-broom and the along-track or push-broom type; a hyperspectral area array; and a digital framing camera. After being focused by a mirror system, in a typical multispectral imager the radiation from each imaged pixel is broken down into spectral bands with one image being produced in each spectral band. The thermal infrared uses primarily the 10 μm atmospheric window. The microwave region contains active radar and passive microwave radiometers (see Fig. 2.1).

2.3 Airborne and Satellite Systems

Which remote sensing platform and sensor data are used depends on the mission requirements. These can be broken down into spatial, spectral, radiometric and temporal. Spatial requirements include the ground resolution (minimum mapping unit) and coverage (swath-width). Spectral requirements include the location, width and number of the spectral bands. For radiometry we must choose the suitable dynamic range and the number of quantization (grey) levels. There are usually between 256 (8-bit) and 4096 (12-bit) quantization levels. The temporal resolution is determined by the required frequency of coverage (i.e. hourly, daily, seasonal), cloud cover, sun
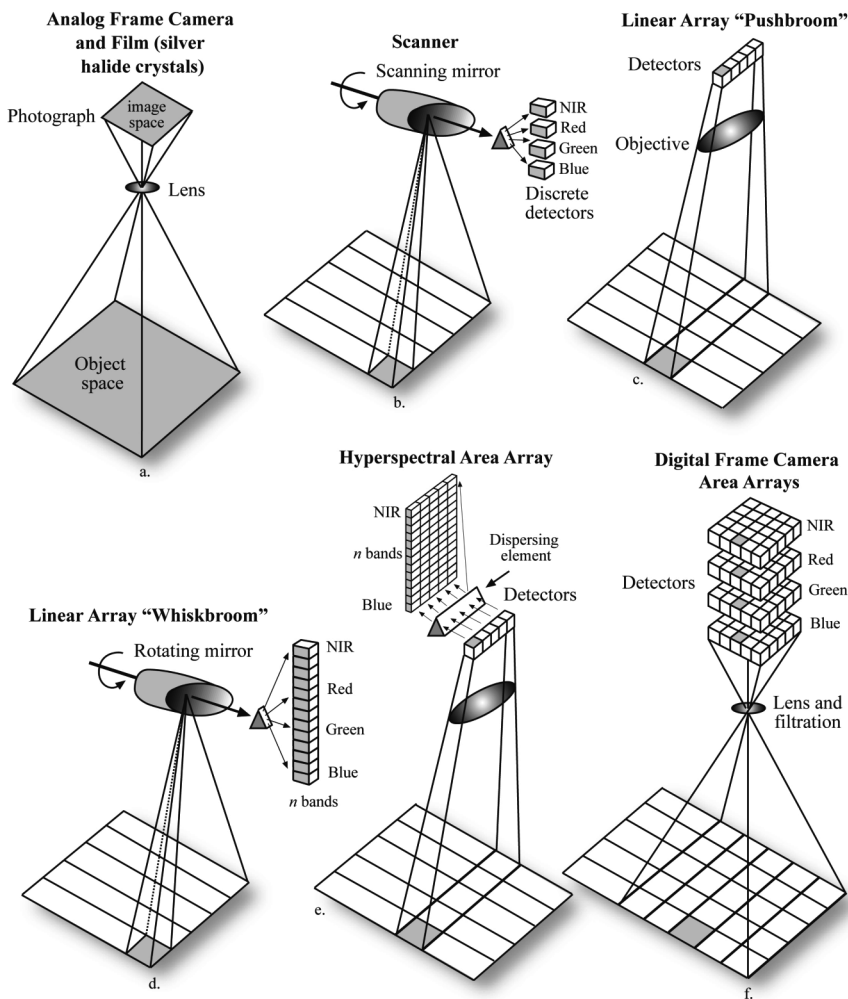
Fig. 2.2 Remote sensing systems used to collect multispectral and hyperspectral imagery (Jensen 2007)

angle and tidal conditions. The general requirements for open ocean, coastal and upland remote sensing are summarized in Table 2.2. As shown, the spatial, spectral, radiometric and temporal resolution requirements are quite different for each of these applications and depend on the specific problem to be solved (Bissett et al. 2004, Jensen 2007).

Remote sensing aircraft are usually flown at high, medium, or low altitudes, depending on the resolution and coverage requirements. High altitude flights covering large regions are normally performed by government agencies, whereas medium altitude flights are often provided by private companies. Low altitude flights may involve small aircraft, sometimes used to supplement field data collection. The tradeoffs one must make in selecting flight altitudes and imaging systems are outlined in

Table 2.2 Remote sensing requirements

	Open ocean	Estuaries	Land
Spatial Resolution	1–10 km	20–200 m	1–30 m
Coverage Area	2000 × 2000 km	200 × 200 km	200 × 200 km
Frequency of Coverage	1–6 days	0.5–6 h	0.5–5 years
Dynamic Range	Narrow	Wide	Wide
Radiometric Resolution	10–12 bits	10–12 bits	8–10 bits
Spectral Resolution	Multispectral	Hyperspectral	Multispectral (Hyperspectral)

Fig. 2.3. For instance, spatial resolution can be traded off for coverage (swath width) by varying the flight altitude or the focal length of the camera's lens system.

There are about 29 civil land imaging satellites in orbit and 34 more are planned. Among these are 18 high-resolution (0.5–1.8 m) and 44 mid-resolution (2–36 m) systems. A list of the more relevant satellites is shown in Table 2.3. Most of these satellites are in polar, sun-synchronous orbits. As the Earth rotates beneath the polar orbiting satellite, its sensors eventually are able to observe and map every part of the globe. The satellite's orbit can also be adjusted to be sun-synchronous, repeating its passes over a site during the same time of day (or same solar illumination angle). Geostationary orbit satellites are stationed above a fixed point on the equator, having the same angular velocity as the Earth, and thus continuously observe the same one third of the Earth's surface. Geostationary satellites provide less spatial resolution
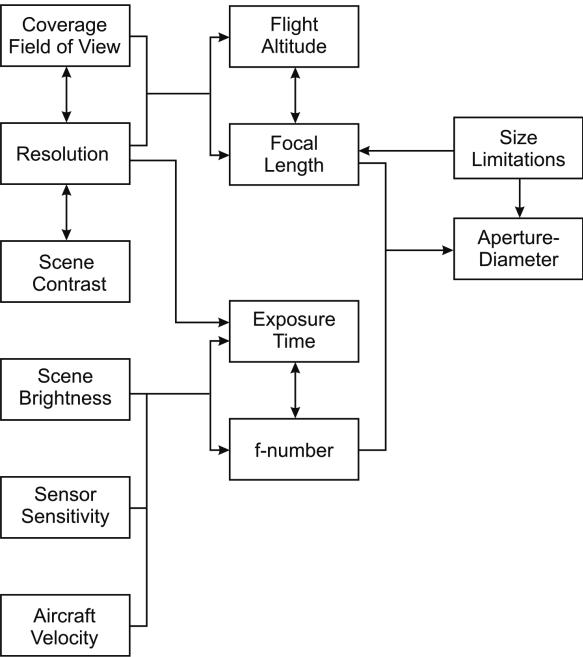

Fig. 2.3 Aerial photography trade-offs

Table 2.3 Coastal zone related sensors on satellite platforms

Satellite	Sensor	Spectral band (μm)		Resolution (m)	Cycle (days)	Swath width (km)
Landsat 1, 2, 3	MSS	4	0.5–0.6	80	18	180
		5	0.6–0.7			
		6	0.7–0.8			
		7	0.8–1.1			
Landsat 4, 5	TM	1	0.45–0.52	30 band 1–6	16	180
		2	0.52–0.60	120 band 7		
		3	0.63–0.69			
		4	0.76–0.90			
		5	1.55–1.75			
		6	2.08–2.35			
		7	10.40–12.50			
Landsat 7	TM	1	0.450–0.514	30 band 1–7	16	180
		2	0.525–0.605	60 band 6		
		3	0.630–0.690	15 band 8		
		4	0.750–0.900			
		5	1.55–1.75			
		6	10.40–12.50			
		7	2.08–2.35			
		8	(Pan) 0.52–0.90			
SPOT	HRV	1	0.50–0.59			
		2	0.61–0.68	20 band 1–3	26 (daily if camera	60
		3	0.79–0.89	10 band 4	tilted)	
		4	0.51–0.73			
IKONOS		1	0.45–0.52			
		2	0.52–0.60	4 band 1–4	< 3 days	11
		3	0.63–0.69	1 band 5		
		4	0.76–0.90			
		5	(Pan) 0.45–0.90			
NOAA	AVHRR	1	0.58–0.68			
		2	0.725–1.1	1,100	2/day	2,400
		3	3.55–3.93			
		4	10.5–11.3			
		5	11.5–12.5			
Orbview 2	SeaWiFS	1	404–422			
		2	433–453	1,100	Daily	2,800
		3	480–500			
		4	500–520			
		5	545–565			
		6	660–680			
		7	745–785			
		8	845–885			

(4–8 km), but have the short repeat cycles needed for tracking storms and weather fronts (every 15–30 min) (Lillesand and Kiefer 1994, Jensen 2007).

Two of the more common medium-resolution satellites for mapping coastal land cover on a regional scale have been the U.S. Landsat and French SPOT (Le Systeme pour l'Observation de la Terre). As shown in Table 2.3, the satellites have multispectral scanners which provide spatial resolutions of 10–30 m and cover swaths from 60 km to 180 km wide. Their repeat cycle, even without cloud cover, is only every 16–26 days. SPOT has the ability to tilt its camera, resulting in a daily repeat cycle and stereo mapping capability.

The medium resolution data from the Landsat and SPOT systems provide information for local or regional studies, but are not quite suitable for investigations at global scales, because of cloud cover and differences in sun angle which prevent convenient comparisons and mosaicking of many scenes into a seamless data set covering a large area.

For global land cover mapping, the NOAA-AVHRR sensors seem to be more efficient, having 2,400 km swath widths and 1.1 km spatial resolutions. Vegetation indices derived from the NOAA-AVHRR sensor have been employed for both qualitative and quantitative studies of forest, desert and other ecosystems, including the contraction and expansion of the Sahara desert, Sellers and Schimel (1993), the calculation of biophysical parameters for climate models, etc. An overview of these studies is given by Prince and Justice (1991), Tucker et al. (1991), and Kogan (2001).

In the late nineties, private satellite companies started collecting high-resolution remote sensing data. The satellites from Space Imaging (IKONOS), Digital Globe (QuickBird) and Orbimage (Orbview-3) are already in orbit capturing imagery at down to 0.6 m resolution. Table 2.4 lists specific information about these satellite systems, including ground resolution, swath width and spectral coverage (Al-Tahir et al. 2006).

Table 2.4 Satellite parameters and spectral bands (Space Imaging 2003, Digital Globe 2003, Orbimage 2003)

		Ikonos	QuickBird	OrbView-3
Sponsor		Space Imaging	Digital Globe	Orbimage
Launched		Sept. 1999	Oct. 2001	June 2003
Spatial	Panchromatic	1.0	0.61	1.0
Resolution (m)	Multi-Spectral	4.0	2.44	4.0
Spectral Range	Panchromatic	525–928	450–900	450–900
(nm)	Blue	450–520	450–520	450–520
	Green	510–600	520–600	520–600
	Red	630–690	630–690	625–695
	Near Infrared	760–850	760–890	760–900
Swath width (km)		11.3	16.5	8
Off nadir pointing		$\pm 26°$	$\pm 30°$	$\pm 45°$
Revisit time (days)		2.3–3.4	1–3.5	1.5–3
Orbital Altitude (km)		681	450	470

As shown in Table 2.4, these systems share several common specifications with respect to spectral and spatial resolution as well as orbital details. (Space Imaging 2003, Digital Globe 2003, Orbimage 2003) Their 11-bit dynamic range allows greater detail to be extracted from scenes that are very dark (e.g. shadows) or very washed out due to excessive sun reflectance. Also, one-meter color imagery can be created using a pan-sharpening process that combines the high spatial resolution of the panchromatic image with the spectral information of the multispectral bands (Read et al. 2003, Souza and Roberts 2005).

In the early 1990s NASA developed a program to acquire the environmental data needed to address specific questions posed by concerns over global environmental change, called Earth Science Enterprise. This initiated a long-term effort to study the total Earth system and the effects of natural and anthropogenic changes on the global environment. One program component is an integrated system of satellites, the Earth Observing System (EOS), designed to provide a continuous stream of data with instruments tailored to answer specific questions for a better understanding of the nature, rates, and consequences of global environmental change (Campbell 2007).

The EOS plan has included over 30 instruments designed to monitor physical and biological components of the Earth. One example of such a satellite mission is Aqua, a satellite launched in 2002. This satellite carried six distinct Earth-observing instruments to measure numerous aspects of the Earth's atmosphere, land, oceans, biosphere, and cryosphere, with a focus on water in the Earth system. The six instruments include the Atmospheric Infrared Sounder (AIRS), the Advanced Microwave Sounding Unit (AMSU-A), the Humidity Sounder for Brazil (HSB), the Advanced Microwave Scanning Radiometer for EOS (AMSR-E), the Moderate-Resolution Imaging Spectroradiometer (MODIS), and the Cloud's and Earth's Radiant Energy System (CERES). Each instrument has unique characteristics and capabilities, and all six serve together to form a powerful package for Earth observations. (Parkinson 2003). The first satellite in the EOS series, Terra, was launched by NASA in 1999 to analyze the dynamic processes of Earth's land, sea and atmosphere. Several of Terra's key sensors, such as the MODIS, are described in Table 2.5.

2.4 Remote Sensing of Coastal Wetlands and Land Cover

Most coastal watershed models require land cover or land use as an input. Knowing how the land cover/use is changing, these models, together with a few other inputs like slope and precipitation, can predict the amount and type of run-off into rivers, bays, and estuaries (Donato and Klemas 2001, Jensen 2007). The Landsat Thematic Mapper (TM) has been a reliable source for land cover data. Its 30 m resolution and spectral bands have proven adequate for observing land cover changes in large coastal watersheds (e.g. Chesapeake Bay). Other similar satellites with medium resolution imagers can also be used, as shown in Table 2.5. The classification schemes used, usually employ the Anderson USGS land cover classification

Table 2.5 Characteristics of some current and scheduled satellite remote sensing systems (From Donato and Klemas 2001)

Satellite/Sensor	Spectral range	Bands	GSD	Revisit time	Swath width	Application
AVHRR NOAA 15/16	580–12500 nm	6	1.1 km	~12h	2400 km	SST, Turbidity, Circulation
SeaWIFS	402–885 nm	8	1.1 km	daily	2800 km	Ocean Color, Red Products
MODIS Terra/Aqua	620–14385 nm	16VNIR 4SWIR 16TIR	250 m – 1 km	daily ~12h	2330 km	SST, Turbidity, Circulation, Ocean Color
MISR Terra (9 Camera angles)	425–886 nm	4	275 m	9d	360 km	Ocean Color, Circulation
ASTER Terra	520–11650 nm	3VNIR 6SWIR 5TIR	15 m 30 m 90 m	16d	60 km	Bathymetry, Vegetation, Land Use, Change Detection, Circulation, Geomorphology
LANDSAT-7	450–2080 nm 10420 nm	6VNIR 1TIR 1 Pan	30 m 60 m 15 m	16d	180 km	
SPOT 1-2-4-5	500–890 nm	3MS 1 Pan	20 m 10 m	26d daily	60 m	
IKONOS	450–750 nm	4MS 1 Pan	4 m 1 m	1–3d	13 km	Bathymetry, Vegetation, Littoral Processes, Digital Elevation models
Quick Bird 2	450–900 nm	4MS 1 Pan	4 m 1 m	<3d	22 km	
Orbview 3	450–900 m	4MS 1 Pan	4 m 1 m	<3d	8 km	
Orbview 4	450–2500 nm 450–900 nm	200HS 4MS 1 Pan	8 m 4 m 1 m	<3d	5 km	

Table 2.5 (continued)

Satellite/Sensor	Spectral range	Bands	GSD	Revisit time	Swath width	Application
ALIEO-1	400–2400 nm	9MS 1 Pan	30 m 10 m	19d	37 km	Bathymetry, Vegetation, Land Use, Change Detection, Circulation, Geomorphology
Hyperion EO-1 NEMO/COIS	400–2400 nm 400–2500 nm	220 210	30 m 30 m	16d	8 km	Bathymetry, Vegetation, Littoral Processes
MERIS ENVISAT-1	290–1040	15	300 m	< 3d	1150 km	Ocean Color, Circulation
ASAR ENVISAT-1	C-band 4 pol	2	30 m	< 3d	50–100 km	Circulation, Waves
AMI ERS-2(SAR)	C-band V pol	1	25 m	28d	100 km	
RADARSAT-1 (SAR)	C-band H pol	1	6–100 m	1–4	20–500 km	
RADARSAT-2 (SAR)	C-band HV pol	1	3–100 m		20–500 km	

system (Anderson et al. 1976) for the top level, and develop their own classification for the more detailed levels, such as the C-CAP Classification System (Klemas et al. 1993, Dobson et al. 1995). A very detailed wetlands classification system is the one developed by Cowardin et al. (1979). However, this classification system proved to be too complex for satellite remote sensing. Some of the ecosystem health indicators that can be observed by remote sensors include percent of impervious areas, natural vegetation cover, buffer degradation, wetland loss and fragmentation, wetland biomass change, invasive species, etc. (Odum 1993, Lathrop et al. 2000, Klemas 2005).

There are numerous approaches to computer-aided image classification (Jensen 1996). A typical digital image analysis approach for classifying coastal wetlands or land cover is shown in Fig. 2.4. Before analysis, the multispectral imagery must be radiometrically and geometrically corrected. The radiometric correction reduces the influence of haze and other atmospheric scattering particles and any sensor anomalies. The geometric correction reorients the image to compensate for the Earth's rotation and for variations in the position and attitude of the satellite. Image segmentation simplifies the analysis by first dividing the image into ecologically distinct areas. Then training sites are identified for supervised classification and interpreted via field visits or other reference data, such as aerial photographs. Next, an
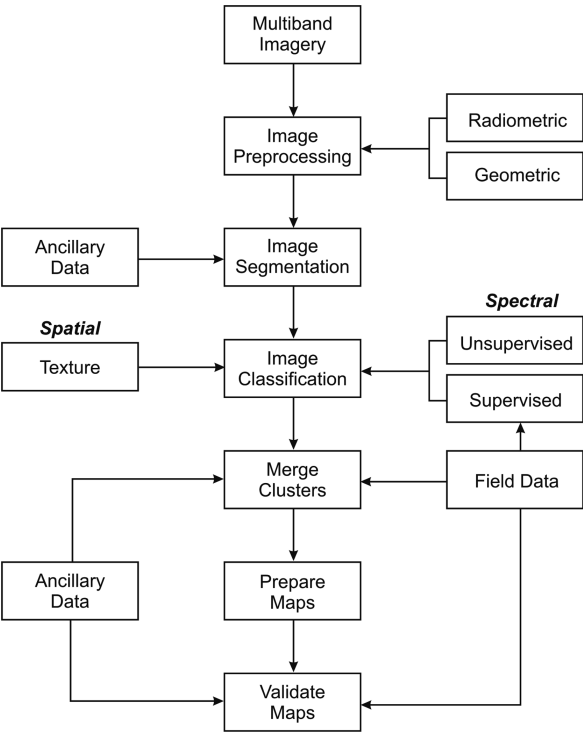

Fig. 2.4 Typical image analysis procedure

unsupervised classification is performed to identify variations in the image not contained in the training sites. Training site spectral clusters and unsupervised spectral classes are then analyzed using cluster analysis to develop an optimum set of spectral signatures. Final image classification is then performed to match the classified themes with the project requirements. (Lachowski et al. 1995, Jensen 1996). Texture analysis is quite useful, but more difficult to automate and is best performed visually (Sabins 1978, Purkis 2005). Note that throughout the process, ancillary data is used, whenever available (e.g. aerial photos, maps, field data, etc.).

When studying critical wetland sites or small watersheds one can use aircraft or high resolution satellite systems. Airborne digital cameras, providing color and color infrared digital imagery are particularly suitable for mapping or validating satellite data. Such digital imagery can be integrated with GPS information and used as georeferenced layers in a GIS for a wide range of modeling applications (Lyon and McCarthy 1995). Small aircraft flown at low altitudes (e.g. 500 m) can be used to supplement field data. High resolution imagery (0.6–4 m) can also be obtained from satellites, such as IKONOS and QuickBird (see Table 2.4). The cost becomes excessive if the site is larger than a few hundred square kilometers. Wetland species identification is difficult; however, some progress is being made using hyperspectral imagers (Schmidt et al. 2004, Porter 2006).

For looking at coastal land cover changes or beach erosion over long time periods, it is important to review historical airphotos, held by local, state and federal agencies. The U.S. Geological Survey and the USDA Soil Conservation Service have useable aerial photos of the coast dating back to the 1930s. They also have various maps, including planimetric, topographic, quadrangle, thematic, orthophoto, satellite and digital maps (Rasher and Weaver 1990, Lachowski et al. 1995). For instance, to map long-term changes of the shoreline due to beach erosion, time series of aerial photographs are used. The shoreline is divided into segments which are uniformly eroding or accreting. Then the change in the distance of the waterline is measured in reference to some stable feature like a coastal highway (Jensen 2007).

The actual beach profile can be obtained with low altitude LIDAR flights. Optical water clarity is the most limiting factor for LIDAR depth detection. Therefore, it is important to conduct the LIDAR overflights during tidal and current conditions that minimize the water turbidity due to sediment resuspension and river inflow. The LIDAR system must have a kd factor large enough to accommodate the water depth and water turbidity at the study site (k = attenuation coefficient; d = water depth). For instance, if a given LIDAR system has a kd = 3 and the turbid water has an attenuation coefficient of k = 1, the system will be effective only to depths of about 3 m. Beyond that depth, one may have to use acoustic echo-sounding techniques (Brock and Sallenger 2000).

Mapping submerged aquatic vegetation (SAV) and coral reefs requires high resolution (1–4 m) imagery (Mumby and Edwards 2002, Purkis 2005). Coral reef ecosystems usually exist in clear water and can be classified to show different forms of coral reef, dead coral, coral rubble, algal cover, sand lagoons, different densities of seagrasses, etc. SAV may grow in more turbid waters and thus is more difficult to map. High resolution (e.g. IKONOS) multispectral imagers have been used in the

past to map SAV and coral reefs; however, hyperspectral imagers should improve the results significantly (Maeder et al. 2002, Mishra et al. 2006).

Digital change detection using satellite imagery can be performed effectively by employing one of several techniques, including post-classification comparison and temporal image differencing (Dobson et al. 1995, Jensen 1996, Lunetta and Elvidge 1998). Post-classification comparison change detection requires rectification and classification of the remotely sensed images from both dates. These two maps are then compared on a pixel-by-pixel basis. One disadvantage is that every error in the individual date classification maps will also be present in the final change detection map.

Temporal image differencing minimizes this problem by performing the traditional classification of only one of the two time-separated images. One band from both dates of imagery is then analyzed to find differences. Pixel intensity difference values exceeding a selected threshold are considered as changed. A change/no change binary mask is overlaid onto the second date image and only the pixels classified as having changed are classified in the second date imagery. This method usually reduces change detection errors and provides detailed from-to change class information (Jensen 1996). As shown in Fig. 2.5, change analysis results can be further improved by including probability filtering, allowing only certain changes and forbidding others (e.g. urban to forest).
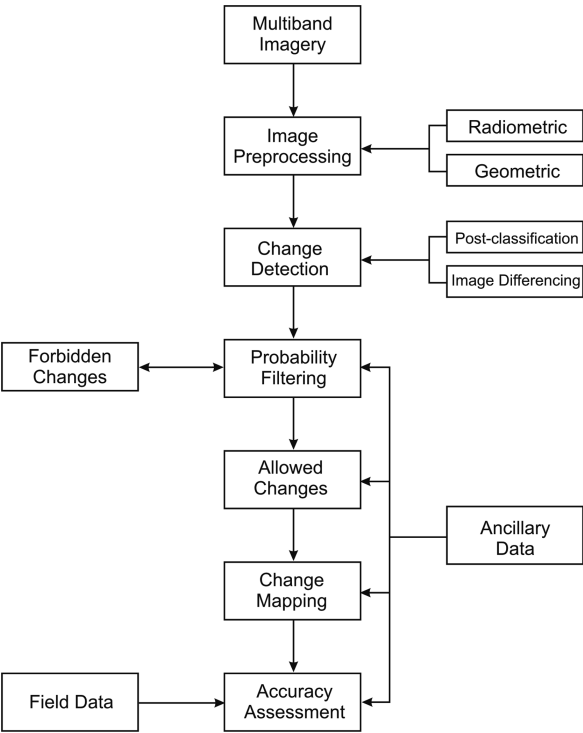

Fig. 2.5 Change detection using probabilities

Biomass and vegetation indices have long been used in remote sensing for monitoring the health and temporal changes associated with wetland or other vegetation (Goward et al. 1991, Lyon and McCarthy 1995). The spectral bands used for biomass mapping are primarily the red band, which is absorbed by the chlorophyll in the upper leaf layers, and a near-infrared band, which is reflected from the inner leaf structure, yet still penetrates several leaf layers and thus provides information on the canopy thickness and density. These spectral bands are combined in the Normalized Difference Vegetation Index (NDVI) to provide an estimate of above-ground wetland plant biomass in grams dry weight per square meter. The NDVI consists of the difference of the near-infrared and red band radiances (digital numbers) divided by their sum (Hardisky et al. 1984, Gross et al. 1987).

A particularly effective method for remotely sensing wetland changes uses biomass as an indicator. To detect biomass changes the Modified Soil Adjusted Vegetation Index (MSAVI) is used with red and near-infrared reflectances derived from Landsat/TM images (Qi et al. 1994). This biomass algorithm is applied to a time series of Landsat/TM images and used with selected thresholds to detect wetland changes. To minimize natural variations between images in the time series (e.g. atmospheric, annual, seasonal, etc.) it is assumed that the relative distribution of biomass in each sub-basin will remain essentially constant over time. Wetland pixels whose MSAVI deviation from the sub-basin mean changes from its previous deviation by more than a selected threshold value are considered as having changed. Threshold selection determines whether many small changes or only the more significant ones are detected. To minimize data costs, only changed sites "flagged" by Landsat/TM are studied in more detail with high-resolution systems, such as IKONOS or airborne scanners (Porter 2006, Klemas 2007).

2.5 Remote Sensing of Coastal and Estuarine Waters

In the open ocean, biological productivity can be estimated by measuring the chlorophyll-a concentration. It is the primary substance determining the color of so-called Case 1 waters, i.e. waters whose color is determined primarily by the chlorophyll concentration, shifting from blue towards green as that concentration increases. Several satellites with multispectral imagers, such as the Coastal Zone Color Scanner (CZCS) and NASA's Sea-viewing Wide Field-of-view Sensor (Sea-WiFS), were specifically designed to map ocean color and sea temperatures on a global scale (Martin 2004, McClain et al. 2006). With the help of calibration data from buoys and ships, these satellites have been able to determine chlorophyll concentrations in the open ocean. Typical ocean color products provided by these and more recent satellites and sensors, such as MODIS, MERIS and AQUA, are shown in Table 2.6 (Arnone and Parsons 2004, Bissett et al. 2004).

The purpose of NASA's Sea-viewing Wide Field-of-view Sensor (SeaWiFS) is to provide quantitative data on global ocean bio-optical properties to biological and physical oceanographers. Subtle changes in ocean color signify various types and

Table 2.6 Ocean color products (Arnone and Parsons 2004)

Chlorophyll concentration	Biological processes such as algal (harmful and non-harmful) blooms and decay
Spectral backscattering coefficient $bb(\gamma)$	90–180° particle scattering linked to concentration, composition, index of refraction of organic (marine) and inorganic (terrigenous) particles, resuspension
Spectral absorption coefficient $a(\lambda)$	Total absorption, changes in water quality
Spectral absorption colored dissolved organic matter $a(CDOM\lambda)$	Conservative tracer of river plumes, linked with coastal salinity, photo-oxidation processes
Spectral particle absorption coefficient $a(p\lambda)$	Particle composition, (organic and inorganic particles)
Spectral phytoplankton absorption coefficient $a(\phi\lambda)$	Absorption linked to differences in chlorophyll packaging within phytoplankton cells
Remote sensing reflectance RRS (λ)	Spectral absolute water color and water signature
Diffuse attenuation coefficient (k532, k490)	Light penetration depth, light availability at depth
Aerosol concentration – Epsilon	Type and distribution, affects visibility, Atmospheric correction methods
Beam attenuation coefficient – $c(\lambda)$	Total light attenuation using a collimated beam
Diver visibility	Horizontal visibility, average target size, target contrast, solar overhead illumination
Laser penetration depth	Underwater performance of lasers (imaging or bathymetry systems)

quantities of marine phytoplankton, the knowledge of which has many scientific and practical applications. The ability to map the color of the world's oceans has been used to estimate global ocean productivity (Longhurst et al. 1995, Behrenfeld and Falkowski 1997), aid in delineating oceanic biotic provinces (Longhurst 1998), and study regional shelf break frontal processes (Ryan et al. 1999, Schofield et al. 2004). As shown in Table 2.5, SeaWiFS has eight spectral bands which are optimized for ocean chlorophyll detection and the necessary atmospheric corrections. The spatial resolution is 1.1 km and the swath width 2,800 km. Due to the wide swath width, the revisit time is once per day. Data in the form of analyzed sea surface temperature and chlorophyll charts are provided daily to the fisheries and shipping industries over Marine Radio Networks. Because certain species of commercial and game fish are indigenous to waters of a specific temperature, fishermen can cut fuel costs and time by being able to locate areas of higher catch potential (Cracknell and Hayes 2007).

Wind-induced upwelling in coastal regions brings nutrients to the surface, creating zones of high biological productivity, accompanied by high concentrations of chlorophyll and phytoplankton, which can be detected by color sensors on satellites. The waters off Peru and California are good examples, where long term upwelling events influence the abundance of fish over periods of months. When wind patterns over the Pacific Ocean change, warm waters from the Western Pacific shift to the

Eastern Pacific and the upwelling of nutrient-rich cold water off the Peruvian coast is suppressed, resulting in well-recognized "El Nino" conditions (Yan et al. 1993). Such upwelling areas and their condition can be observed by satellites with thermal infrared imagers, such as NOAA's AVHRR, or ocean color sensors, such as Sea-WiFS (Schofield et al. 2004, Martin 2004).

As one approaches the coast and enters the bays and estuaries, the water becomes quite turbid and contains suspended sediment, dissolved organics and other substances, in addition to chlorophyll. To identify each substance in this complex mixture of Case 2 waters requires hyperspectral sensors and more sophisticated algorithms than the empirical regression models (Sydor 2006, Cannizzaro and Carder 2006) used in Case 1 waters in the open ocean (Ikeda and Dobson 1995, Bukata 2005). Neural network approaches have been used to map chlorophyll and suspended sediment concentrations in Delaware Bay and other estuaries (Keiner and Brown 1999, Dzwonkowski and Yan 2005a). Neural networks, however, require extensive calibration with coincident ship and satellite observations of radiance, and shipboard measurements of chlorophyll and sediment concentrations.

There are many other coastal and estuarine pollutants and ecosystem health indicators that can be sensed by remote sensors. However, to fully understand the behavior and environmental impact of water pollutants such as oil spills or chemical dumps, one usually needs to measure the following parameters:

- source (point, distributed, surface, subsurface)
- location (within permit zone)
- movement (currents, wind, waves, etc.)
- dispersion (density, thermocline, currents, waves, wind, etc.)
- identity (spectral signature)
- condition (weathering, decomposition, etc.)
- concentration (ambient, source, surface, subsurface, etc.)
- environmental impact (animals, plants, beaches, water quality, etc.)

Most of these pollution characteristics can be sensed remotely, especially if hyperspectral imagers having adequate spatial resolution are employed.

High concentrations of nutrients exported from agriculture or urban sprawl in coastal watersheds, or produced by coastal upwelling, are causing harmful algal blooms in many estuaries and coastal waters. Algal blooms are harmful in that they cause eutrophic conditions, depleting oxygen levels needed by organic life and limiting aquatic plant growth by reducing water transparency. Most algal blooms can be observed from satellites, due to their distinct color, location or repetitive seasonal appearance (Ruddick 2001). Furthermore, hyperspectral sensors with spectral bands fine-tuned for specific pigment analysis allow detection and analysis of algal taxonomy. This can be accomplished because the species-specific algal accessory pigments produce unique spectral signatures. Remote sensing data can complement the monitoring networks existing in many parts of the world to get data on nutrient loading and algal growth to provide better insights into overall water quality, distribution of toxin-producing algae, and aquatic biogeochemical cycling (Gitelson 1993).

Table 2.7 Water quality levels

Water quality	Chl-a concentration
Oligotrophic	$< 8\,\mu g/L$
Mesotrophic	8–$25\,\mu g/L$
Eutrophic	$> 25\,\mu g/L$
Water quality	**Total Suspended Sediment (TSS)**
Clear	0–$10\,mg/L$
Moderately turbid	10–$50\,mg/L$
Highly turbid	$> 50\,mg/L$
Examples	Delaware Bay is mesotrophic and moderately to highly turbid
	Chesapeake Bay is mesotrophic to eutrophic and moderately turbid

Concentrations of chlorophyll-a (chl-a) and total suspended sediments (TSS) can be sensed remotely and used as indicators of the severity of eutrophication and turbidity, respectively. If such general criteria, as shown in Table 2.7, are used to compare estuarine water quality, it is possible to get satisfactory results with sensors having fewer spectral bands and lower signal to noise ratios than the hyperspectral imagers needed for measuring precise concentration levels (Chipman et al. 2004).

Most riverine and estuarine plumes and some ocean-dumped waste plumes can be detected remotely due to their strong surface signatures caused by high turbidity. The drift and dispersion of coastal plumes and ocean dumped waste have been tracked with satellite imagery. (Klemas and Philpot 1981, Dzwonkowski and Yan 2005b, Thomas and Weatherbee 2006). To study the dynamics of such plumes one can use a small number of multispectral bands. However, to detect the composition and concentration of their content is difficult, even with hyperspectral images.

Some studies of coastal ecosystems require physical data as well as biological information. As shown in Table 2.8, radar and thermal infrared sensors are available on aircraft and satellites for measuring and mapping the physical properties of coastal and estuarine waters. Surface and internal wave fields as well as oil slicks can be mapped with radar imagers, such as the Synthetic Aperture Radar (SAR) mounted on satellites. Radar altimeters provide accurate sea surface height as well

Table 2.8 Space-borne ocean-sensing techniques

Sensing technique	Environmental parameters
Color Scanner –	Ocean Color (chlorophyll concentration, suspended sediment, attenuation coefficient)
Infrared Radiometer –	Sea surface temperature (surface temperature, current patterns)
Synthetic Aperture Radar –	Short surface waves (swell, internal waves, oil slicks, etc.)
Altimeter –	Topography and roughness of sea surface (sea level, currents, wave height)
Scatterometer –	Amplitude of short surface waves (surface wind velocity, roughness)
Microwave Radiometer –	Microwave brightness temperature (salinity, surface temp., water vapor, soil moisture)

as wave amplitude information. Radar scatterometer data can be analyzed to extract sea surface winds. (Martin 2004, Elachi and van Ziel 2006). The two passive devices, microwave radiometers and thermal infrared scanners can sense sea surface salinity and temperature, respectively. Microwave radiometers can also measure a wide range of climate related parameters, such as soil moisture (Parkinson 2003, Burrage et al. 2003).

Oil spills are best detected by imaging radars, such as SAR on satellites, because oil slicks dampen small surface wavelets, which otherwise backscatter a strong radar return signal. Small aircraft can be used to verify oil spill drift and dispersion models by tracking the movement and spreading of oil slicks in coastal waters and their interactions with fronts. A typical estuarine front may be caused by flooding higher density ocean water gliding under the lower density, lower salinity river water and thus causing a strong convergence zone, which may be marked by a foam line and color line. Estuarine fronts are narrow features, quite dynamic and have high convergence velocities (Sarabun 1993). Coastal and estuarine fronts can concentrate nutrients, pollutants and capture oil slicks causing their paths to deviate from drift and dispersion model predictions (Klemas 1980). To study frontal dynamics and track oil slicks one needs spatial and temporal resolutions of 10–50 m and 0.5–3 h, respectively.

Currents and breaking waves strongly affect coastal ecosystems, especially in the nearshore, which is an extremely dynamic environment. Currents influence the drift and dispersion of various pollutants, and together with breaking waves mobilize and transport sediments, resulting in erosion and morphological evolution of natural beaches. Changes in the underlying bathymetry in turn affect the wave and current patterns, resulting in a feedback mechanism between the hydrodynamics and morphology. The ability to monitor these processes is necessary in order to understand and predict the changes that occur in the nearshore region. Arrays of current meters, acoustic Doppler velocimeters, and pressure sensors are not very effective for determining surface currents and waves over large coastal regions, since these sensors measure currents at a point and are expensive, when large numbers of sensors have to be deployed.

Shore-based high frequency (HF) and microwave Doppler radar systems are used to map currents and determine swell-wave parameters in coastal waters with considerable accuracy. (Paduan and Graber 1997, Graber et al. 1997, Bathgate et al. 2006). The surface current measurements use the concept of Bragg scattering from a slightly rough sea surface, modulated by Doppler velocities of the surface currents. Extraction of swell direction, height and period from HF radar data is based on the modulation imposed on the short Bragg wavelets by the longer faster moving swell. HF radars can determine coastal currents and wave conditions over a range of up to 200 km. (Cracknell and Hayes 2007). While HF radar provides accurate maps of surface currents and wave information for large coastal areas, their spatial resolution, which is about 1 km, is more suitable for measuring mesoscale features than small scale currents. On the other hand, shore-based microwave X-band and S-band radars have resolutions of the order of 10 m, yet have a range of only a few kilometers.

Estimates of currents over large coastal areas, such as the continental shelf, can also be obtained by tracking the movement of drogues, dyes or natural surface features which differ detectably in color or temperature from the background waters (Davis 1985, Breaker et al. 1994). Examples of such features include sediment or chlorophyll plumes, patches of different water temperature, surface slicks, coastal fronts, etc.

Large ocean internal waves on continental shelves strongly influence acoustic wave propagation; submarine navigation; mixing nutrients to euphotic zone; sediment resuspension; cross-shore pollutant transport; and coastal engineering and oil exploration. Internal waves move along pycnoclines, which are surfaces that separate water masses of different densities. The water column is frequently not homogeneous, but stratified, containing thermoclines and pycnoclines that mark boundaries between water masses. The periods of internal waves are measured in minutes, rather than in seconds, and their wavelengths in kilometers rather than in tens of meters. Furthermore, the larger internal waves can attain heights of 100 m (Alford 2003). The period of the internal wave packets approximates the period of the tides, suggesting a cause-and-effect relationship. Internal waves can be detected visually and by radar since they cause local currents which modulate surface wavelets and slicks (Zhao et al. 2004).

Oil tankers, cargo ships, pleasure craft and military vessels navigating in bays such as Delaware Bay or Chesapeake Bay and further north, require information on the extent and type of ice cover during winter months. Types of ice cover may include fast ice, pack ice, large drift ice, small drift ice, etc. Radar and multispectral visible bands can provide such information.

The devastating effects of Atlantic hurricanes and tsunamis in the Indian Ocean bring out the need for timely monitoring of coastal flooding. There are many other storm events, such as Nor'easters, that impact the Atlantic coast more frequently than hurricanes. A good example of a major coastal flooding event is the Nor'easter storm of 1962 (Mather et al. 1967). The waves and storm surge broke through the dune line, flooded the entire coastal zone and damaged boardwalks and homes in settlements along the mid-Atlantic coast. The extensive damage and flooding along the coast was captured in aerial photographs after the storm.

Obtaining images before and after the landfall of hurricane Katrina in New Orleans in 2005, Landsat TM effectively showed the wetland losses and inundation over the entire region at 30 m resolution, while high resolution satellites, like IKONOS and QuickBird, documented the details, including actual breaks in the levees protecting the city. However, more frequent repeat cycles would have been useful for emergency operations. Only SAR could penetrate the clouds to observe coastal inundation conditions during the time of the hurricane's landfall. Radar can detect flooded coastal marshes because they usually provide a weaker radar return than non-flooded ones. The marsh grasses may calm the water surface accentuating specular reflection (Ramsey 1995). The radar return from flooded forests is usually enhanced compared to returns from nonflooded forests. The enhancement is due to the double bounce mechanism where the signal penetrating the canopy is reflected off the water surface and subsequently reflected back toward the sensor by a second reflection off a tree trunk (Hess et al. 1990).

2.6 Field Data

Field or ship data need to be collected for developing a spectral "signature library" for supervised classification of land cover, calibrating remotely sensed data or training neural networks. Field checks may also have to be conducted in order to guide the interpreters during the image classification stage. Finally, field data is gathered at the end of a project to validate the remotely sensed products (e.g. wetland maps) and assess their accuracy.

Training sites for supervised classification of coastal land cover must meet well-defined criteria. They should be homogeneous with regard to vegetation/land cover and in accessible areas. They should be large enough so they can be located on satellite images, but small enough to minimize within-site variation (10–25 pixels in size). Multiple training sites for each category of the classification scheme are required. (e.g. 10 sites).

To determine the reflectance characteristics of a land surface, a goniometer can be used to measure the Bidirectional Reflectance Distribution Function (BRDF). This is a tedious procedure, requiring that the irradiance and radiance be measured at all sensor positions and all solar angles. A more practical way is to compare the site's reflectance with that of a Lambertian white panel (diffuse reflector) made of special materials, such as Halon, having controlled reflectivities from 95% to 99% (McCoy 2005, Jensen 2007). To convert ground reflectances to at-satellite-reflectances, one can use large white canvas sheets or natural targets large enough to be identifiable in the satellite imagery and having reflectances covering the entire range of the reflectances of the land cover sites to be mapped. (e.g. a corn field, a large lawn, a field of dry soil, etc.). By measuring the reflectances of these targets on the ground and at the satellite, and comparing them with the Lambertian white (Halon) panels, one can calibrate the satellite sensor so it could measure the reflectances of all the pixels in the scene (Gross et al. 1987).

To validate the remote sensing results and determine their accuracy, a statistically valid sampling scheme should be selected. For instance, for land cover maps a systematic unaligned sampling pattern is frequently used. On the other hand, some situations may require a clustered or stratified random sampling pattern. Tests by various researchers have shown the simple random and stratified random patterns both give satisfactory results. However, the stratified random approach requires some advance knowledge of where the land cover boundaries are located (McCoy 2005).

The accuracy of completed map products can be expressed in terms of an error matrix for land cover mapping applications and as percentage error for water quality studies. Furthermore, a Kappa coefficient can be calculated to show how much better the map results are than a totally random labeling of the pixels in the image (Jensen 1996, Campbell 2007).

Instrumented ships, buoys, and ocean gliders are used to calibrate and validate chlorophyll-a and total suspended sediment maps obtained with multispectral ocean color sensors. Some typical ship or buoy measurements are shown in Table 2.9. In coastal and estuarine waters this data must frequently be obtained very close to the

Table 2.9 Remote sensing related ship measurements

Direct measurements

Temperature, Salinity, Secchi Depth, pH, Attenuation Coefficient, Spectral Reflectance
   (Radiance and Irradiance)

Water sample analysis

Chl-a, TSS, Nitrogen, Phosphorus

Ship data acquisition

Water samples obtained from upper 0.5 m of water column; Ship data obtained within 20 min of
   satellite overpass; GPS used for sample site location

---

satellite overpass time and be statistically representative of prevailing conditions.
The water samples are usually taken from the upper half meter of the water column.
Sites for calibrating remotely sensed data, such as chlorophyll concentrations in
coastal waters, must be located at well-known points representing the entire range
of variables to be measured.

2.7 Summary and Conclusions

Since the early 1970s, civilian remote sensing satellites have made major contri-
butions to our understanding of the Earth's ecosystems and warned us of critical
natural and man-made changes taking place, such as deforestation, desertification
and shrinking glaciers in Greenland and the Antarctic. In the open ocean, satellites
have tracked storms and major oil spills. They have also monitored fisheries-related
chlorophyll concentrations, algal blooms and sea surface temperatures. However,
obtaining this information for coastal and estuarine ecosystems is more challeng-
ing, since they exhibit extreme variations in spatial complexity and temporal vari-
ability. After several decades of improvements, it now appears that remote sensing
needs, cost and technology are converging in a way that will prove practical and
cost-effective for coastal managers and ecosystem researchers. A few specific con-
clusions and recommendations are outlined below:

- As shown in Table 2.2, remote sensing of coastal ecosystems requires high spa-
  tial, spectral, and temporal resolution.
- Aerial photography of coastal ecosystems is usually performed at medium al-
  titudes with color film, color infrared film and digital cameras at scales of
  1:1,200–1:24,000. Large coastal regions can be mapped from high altitudes
  (scale 1:100,000), while low altitude flights (scale 1:600) can be used in support
  of field data collection (Jensen 2007, Campbell 2007).
- Georeferenced orthophotos, topographic maps and land cover maps represent
  good base maps for creating a multi-layer GIS database. Digital camera images
  are especially suited for use with GIS databases and for interpreting land cover
  maps derived from satellite imagery (Porter 2006).

- To keep costs reasonable, large coastal watersheds should be studied with medium resolution satellite sensors (e.g. 30 m Landsat TM) and only small areas and critical sites mapped with airborne or high resolution satellite sensors (e.g. 1–4 m IKONOS).
- For detecting changes of coastal land cover, including tidal marshes, in a time-series of images, post-classification comparison, image differencing and biomass change techniques can be used. To determine man-made changes, the images must be corrected for natural variations such as atmospheric, inter-annual, seasonal, and tidal differences (Lunetta and Elvidge 1998).
- On land, field data are often collected along transects using systematic random sampling. The sampling scheme should be optimized for each type of image classification approach, e.g. supervised, unsupervised, etc. (McCoy 2005, Jensen 1996).
- Mapping wetlands, coral reefs and submerged aquatic vegetation requires high resolution (1–4 m) imagery. Wetland species identification is possible only with hyperspectral sensors and large amounts of field data (Klemas 2005, Mumby and Edwards 2002, Schmidt et al. 2004).
- Airborne LIDAR is effective for near-shore bathymetry, but in turbid waters when the kd product exceeds the vendor specified value, acoustic echo sounding techniques must be used (k = attenuation coefficient; d = depth) (Brock and Sallenger 2000).
- Coastal and estuarine waters contain a complex mixture of chlorophyll, suspended sediments, dissolved organics, and other substances. Therefore, hyperspectral imagers, calibrated ship data and advanced algorithms or neural network methods are required to map the concentrations of these substances (Ikeda and Dobson 1995).
- Approximate concentrations of chl-a and total suspended sediments can be obtained with multispectral scanners and a small number of ship samples.
- Ship samples and water reflectances must be gathered very close to satellite over-pass times. Spotter planes can be used to guide the research vessels to water features of interest.
- Thermal infrared radiometers or imagers, such as the AVHRR on NOAA satellites, can map sea surface temperature to within $0.5\,^{\circ}$C accuracy.
- Radar altimeters, scatterometers and SAR imagers can be used for mapping sea level height, sea surface winds, waves and currents (Ikeda and Dobson 1995, Martin 2004).

References

Alford MH (2003) Redistribution of energy available for ocean mixing by long-range propagation of internal waves. Nature 423:159–162

Al-Tahir A, Baban SMJ, Ramlal B (2006) Utilizing emerging geo-imaging technologies for the management of tropical coastal environments. West Indian J Eng 29:11–22

Anderson JR, Hardy EE, Roach JT, Witmer RE (1976) A land use and land cover classification system for use with remote sensor data. US Geological Survey Professional Paper 964, Washington, DC, 28p

Arnone RA, Parsons AR (2004) Real-time use of ocean color remote sensing for coastal monitoring. In: Miller RL, Del Castillo CE, McKee BA (eds) Remote sensing of the coastal environment. Springer Publishing, Kluwer Academic, New York

Avery TE, Berlin GL (1992) Fundamentals of remote sensing and airphoto interpretation. Macmillan, New York

Bathgate J, Heron M, Prytz A (2006) A method of swell parameter extraction from HF ocean surface radar spectra. IEEE J Oceanic Eng 31:812–818

Behrenfeld MJ, Falkowski PG (1997) Photosynthetic rates derived from satellite-based chlorophyll concentration. Limnol Oceanogr 42:1–20

Bissett WP, Arnone R, Davis CO, Dye D, Kohler DDR, Gould R (2004) From meters to kilometers-a look at ocean color scales of variability, spatial coherence, and the need for fine scale remote sensing in coastal ocean optics. Oceanography 17:32–43

Breaker LC, Krasnopolski VM, Rao DB, Yan X-H (1994) The feasibility of estimating ocean surface currents on an operational basis using satellite feature tracking methods. Bull Am Meteor Soc 75:2085–2095

Brock J, Sallenger A (2000) Airborne topographic LIDAR mapping for coastal science. U.S. Geological Survey, Open-File Report 01–46

Bukata R (2005) Satellite monitoring of inland and coastal water quality: retrospection, introspection, future directions. Taylor & Francis, London

Burrage DM, Heron ML, Hacker JM, Miller JL, Stieglitz TC, Steinberg CR, Prytz A (2003) Structure and influence of tropical river plumes in the Great Barrier reef: Application and performance of an airborne sea surface salinity mapping system. Remote Sens Envir 85:204–220

Campbell JB (2007) Introduction to remote sensing. The Guilford Press, New York

Cannizzaro JP, Carder KL (2006) Estimating chlorophyll-a concentrations from remote sensing reflectance in optically shallow waters. Remote Sens Envir 101:13–24

Chipman JW, Lillesand TM, Schmaltz JE, Leale JE, Nordheim MJ (2004). Mapping lake water clarity with Landsat images in Wisconsin, USA. Can J Remote Sens 30:1–7

Cowardin L, Carter V, Golet F, LaRoe E (1979) Classification of wetlands and deep water habitats of the United States. US Department of the Interior, Fish and Wildlife Service, Office of Biological Services, FWS/OBS-79/31. Washington, DC, 131p

Cracknell AP, Hayes L (2007) Introduction to remote sensing. CRC Press, New York

Davis RE (1985) Drifter observations of coastal surface currents during CODE: the method and descriptive view. J Geophys Res 90:4741–4755

Digital Globe (2003) Quickbird imagery products and product guide (revision 4). Digital Globe, Inc., Colorado, USA

Dobson JE, Bright EA, Ferguson RL, Field DW, Wood LL, Haddad KD, Iredale H, Jensen JR, Klemas V, Orth RJ, Thomas JP (1995) NOAA Coastal Change Analysis Program (C-CAP): Guidance for regional implementation, NOAA Technical Report NMFS 123, U.S. Department of Commerce, Washington, DC

Donato T, Klemas V (2001) Remote sensing and modeling applications for coastal resource management. Geocarto Int 16:23–29

Dzwonkowski B, Yan X-H (2005a) Development and application of a neural network based ocean color algorithm in coastal water. Int J Remote Sens 26:1175–1200

Dzwonkowski B, Yan X-H (2005b) Tracking of a Chesapeake Bay estuarine outflow plume with satellite-based ocean color data. Continental Shelf Res 25:1942–1958

Elachi C, van Ziel J (2006) Introduction to the physics and techniques of remote sensing. John Wiley & Sons, New Jersey

Gitelson A (1993) Quantitative remote sensing methods for real-time monitoring of inland water quality. Int J Remote Sens 14:1269–1295

Goward SN, Markham B, Dye DG, Dulaney W, Yang J (1991) Normalized Difference Vegetation Index measurements from the Advanced Very High Resolution Radiometer. Remote Sens Envir 35:257–277

Graber H, Haus B, Chapman R, Shay L (1997) HF radar comparisons with moored estimates of current speed and direction: expected differences and implications. J Geophys Res 102:18, 749–18, 766

Gross MF, Hardisky MA, Klemas V, Wolf PL (1987) Quantification of biomass of the marsh grass Spartina Alterniflora Loisel using Landsat Thematic Mapper imagery. Photogramm Eng Remote Sens 53:1577–1583

Hardisky MA, Daiber FC, Roman CT, Klemas V (1984) Remote sensing of biomass and annual net aerial productivity of a salt marsh. Remote Sens Envir 16:91–106

Hess L, Melack J, Simonett D (1990) Radar detection of flooding beneath the forest canopy: a review. Int J Remote Sens 11:1313–1325

Ikeda M, Dobson FW (1995) Oceanographic applications of remote sensing. CRC Press, New York

Jensen JR (1996) Introductory digital image processing: a remote sensing perspective. Prentice-Hall, New Jersey

Jensen JR (2007) Remote sensing of the environment: an Earth resource perspective. Prentice Hall, New Jersey

Keiner LE, Brown CW (1999) Estimating oceanic chlorophyll concentrations with neural networks. Int J Remote Sens 20:189–194

Kerr JT, Ostrovsky M (2003) From space to species: ecological applications of remote sensing. Trends Ecol Evol 18:299–305

Klemas V (1980) Remote sensing of coastal fronts and their effects on oil dispersion. Int J Remote Sens 1:11–28

Klemas V (2005) Remote sensing: Wetlands classification. In: Schwartz ML (ed) Encyclopedia of coastal science. Springer, Dordrecht, The Netherlands, pp 804–807

Klemas V (2007) Remote sensing of coastal wetlands and estuaries. Proc of Coastal Zone 07. NOAA Coastal Services Center, Charleston, South Carolina

Klemas V, Dobson JE, Ferguson RL, Haddad KD (1993) A coastal land cover classification system for the NOAA Coastwatch Change Analysis Project. J Coast Res 9:862–872

Klemas V, Philpot W (1981) Drift and dispersion studies of ocean-dumped waste using Landsat imagery and current drogues. Photogram Eng Remote Sens 47:533–542

Kogan FN (2001) Operational space technology for global vegetation assessment. Bull Amer Meteor Soc 82:1949–1964

Lachowski H, Maus P, Golden M, Johnson J, Landrum V, Powell J, Varner V, Wirth T, Gonzales J, Bain S (1995) Guidelines for the use of digital imagery for vegetation mapping. U.S. Department of Agriculture, Forest Service EM-7140-25, Washington, DC

Lathrop RG, Cole MB, Showalter RD (2000) Quantifying the habitat structure and spatial pattern of New Jersey (USA) salt marshes under different management regimes. Wetl Ecol Manag 8:163–172

Leica (2002) ADS40 Airborne digital sensor. Leica Geosystems, GIS and Mapping, LLC, Atlanta, Georgia, USA

Lillesand TM, Kiefer RW (1994) Remote sensing and image interpretation. John Wiley & Sons, New Jersey

Longhurst A (1998) Ecological Geography of the Sea. Academic Press, London

Longhurst A, Sathyendranath S, Platt T, Caverhill C (1995) An estimate of global primary production in the ocean from satellite data. J Plank Res 17:1245–1271

Lunetta RS, Elvidge CD (1998) Remote sensing change detection: environmental monitoring methods and applications. Ann Arbor Press, Michigan

Lyon JG, McCarthy J (1995) Wetland and environmental applications of GIS. Lewis Publishers, New York

Maeder J, Narumalani S, Rundquist D, Perk R, Schalles J, Hutchins K, Keck J (2002) Classifying and mapping general coral reef structure using Ikonos data. Photogram Eng Remote Sens 68:1297–1305

Martin S (2004) An introduction to remote sensing. Cambridge University Press, Cambridge

Mather JR, Field RT, Yoshioka GA (1967) Storm damage hazard along the East Coast of the United States. J Appl Meteor 6:20–30

McClain C, Hooker S, Feldman G, Bontempi P (2006) Satellite data for ocean biology, biogeo-chemistry, and climate research. Eos, Transactions, Amer Geophys Union 87:337–343

McCoy R (2005) Field methods in remote sensing. Guilford Press, New York

Mishra D, Narumalani S, Rundquist D, Lawson M (2006) Benthic habitat mapping in tropi-cal marine environments using QuickBird multispectral data. Photogram Eng Remote Sens 72:1037–1048

Mumby PJ, Edwards AJ (2002) Mapping marine environments with Ikonos imagery: enhanced spatial resolution can deliver greater thematic accuracy. Remote Sens Envir 82:248–257

Odum EP (1993) Ecology and Our Endangered Life-Support Systems, 2nd edn. Sinauer Asso-ciates, Inc., Sunderland, MA

Orbimage (2003) OrbView-3 Satellite and ground systems specifications. Orbimage Inc., Vir-ginia, USA

Paduan JD, Graber HC (1997) Introduction to high-frequency radar: Reality and myth. Oceanog-raphy 10:36–39

Parkinson CL (2003) Aqua: An earth-observing satellite mission to examine water and other cli-mate variables. IEEE T Geosci and Remote 41:173–183

Porter DE (2006) RESAAP/Final Report, NOAA/NERRS Remote sensing applications assessment project. University of South Carolina

Prince SD, Justice CO (1991) Coarse resolution remote sensing of the Sahelian environment. Int J Remote Sens 12:1133–1421

Purkis SJ (2005) A reef-up approach to classifying coral habitats from IKONOS imagery. IEEE T Geosci Remote 43:1375–1390

Qi J, Chehbouni A, Huete AR, Kerr YH, Sorooshian S (1994) A modified soil adjusted vegetation index. Remote Sens Envir 48:119–126

Ramsey E (1995) Monitoring flooding in coastal wetlands by using radar imagery and ground-based measurements. Int J Remote Sens 16:2495–2502

Rasher ME, Weaver W (1990) Basic photo interpretation: a comprehensive approach to interpreta-tion of vertical aerial photography for natural resource applications. U.S. Department of Agri-culture, Washington, DC

Read JM, Clark DB, Venticinque EM, Moreira MP (2003) Application of merged 1-m and 4-m resolution satellite data to research and management in tropical forests. J Appl Ecol 40:592–600

Ruddick KG (2001) Optical remote sensing of chlorophyll-a in case 2 waters by use of an adaptive two-band algorithm with optimal error properties. Appl Optics 40:3575–3585

Ryan JP, Yoder JA, Cornillon PC, Barth JA (1999) Chlorophyll enhancement and mixing associ-ated with meanders of the shelf break front in the Mid-Atlantic Bight. J Geophys Res 104:23, 479–23, 493

Sabins FF (1978) Remote sensing: principles and interpretation, 2nd edn. Freeman & Co, New York

Sarabun CC (1993) Observations of a Chesapeake Bay tidal front. Estuaries 16:68–73

Schmidt KS, Skidmore AK, Kloosterman EH, Van Oosten H, Kumar L, Janssen JAM (2004) Map-ping coastal vegetation using an expert system and hyperspectral imagery. Photogram Eng Re-mote Sens 70:703–716

Schofield O, Arnone RA, Bissett WP, Dickey TD, Davis CO, Finkel Z, Oliver M, Moline MA (2004) Watercolors in the Coastal Zone: What can we see? Oceanography 17:25–31

Sellers PJ, Schimel D (1993) Remote sensing of the land biosphere and biochemistry in the EOS era: science priorities, methods of implementation – EOS biosphere and biochemical panels. Global Planet Change 7:279–297

Souza CM, Roberts DA (2005) Mapping forest degradation in the Amazon region with Ikonos images. Int J Remote Sens 26:425–429

Space Imaging (2003) IKONOS Imagery products and product guide (version 1.3). Space Imaging LLC., Colorado, USA

Sydor M (2006) Use of hyperspectral remote sensing reflectance in extracting the spectral volume absorption coefficient for phytoplankton in coastal water: remote sensing relationships for the inherent optical properties of coastal water. J Coastal Res 22:587–594

Thomas AC, Weatherbee RA (2006) Satellite-measured temporal variability of the Columbia River
     plume. Remote Sens Envir 100:167–178
Tucker CJ, Dregne HE, Newcomb WW (1991) Expansion and contraction of the Saharan desert
     from 1980 to 1990. Science 253:299–301
Yan X-H, Ho C, Zheng Q, Klemas V (1993) Using satellite IR in studies of the variabilities of the
     Western Pacific Warm Pool. Science 262:440–441
Zhao X, Klemas V, Zheng Q, Li X, Yan X-H (2004) Estimating parameters of a two-layer stratified
     ocean from polarity conversion of internal solarity waves observed in satellite SAR images.
     Remote Sens Envir 94:276–287